

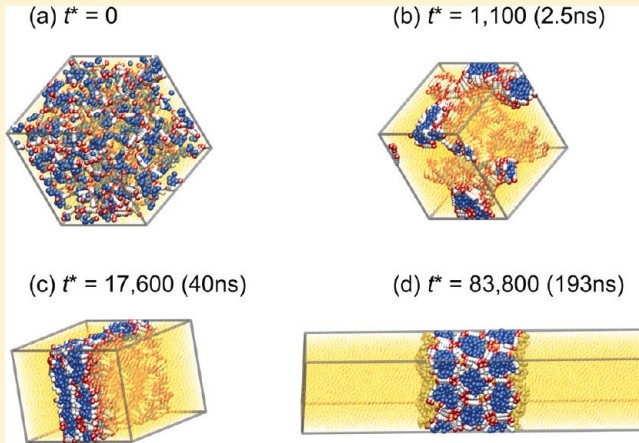
Self-Assembly of T-Shaped Polyphilic Molecules in Solvent Mixtures

Andrew J. Crane and Erich A. Müller*

Department of Chemical Engineering, Imperial College London, U.K.

 Supporting Information

ABSTRACT: Coarse-grained molecular simulations of a model of a T-shaped polyphilic molecule in the presence of solvents are presented. The target molecules are liquid crystal bolaamphiphiles with grafted lateral side chains. The main core of the molecule corresponds to a rigid biphenyl unit, decorated at both ends with polar associating sites. A lateral flexible chain, whose character is mostly antagonistic with respect to the rest of the molecule, imparts unique self-assembly behavior to the pure fluid. In the case herein, the pure T-shaped bolaamphiphile (TsB) forms two-dimensional honeycomb-like columnar structures, and a study is performed on the effects of solvents added to this structure. Three model solvents are considered, each corresponding to the three different parts of the original molecule. We consider the whole concentration range and a temperature at which the pure TsB fluid shows a columnar liquid crystal behavior. All three solvents show different progressions and equilibrium mesophases. The solvent compatible with the end groups swells the structure at low concentrations and at higher concentrations forces a phase split between an essentially pure solvent phase and a structured LC phase. The solvent affine with the core of the TsB does not swell the structure at low concentrations. At higher concentrations, this solvent induces a phase separation where the TsB-rich phase forms a unique liquid crystal membrane. The solvent compatible with the lateral chain will not form stable phase separations, but transforms the columnar structure into a loose, worm-like micellar network. The results reported are generic in nature and describe the phase space for the entire family of TsB's.



1. INTRODUCTION

In recent decades, a great deal of effort has been placed on understanding the complex mesostructures formed by self-assembling macromolecules. Although self-assembly of large molecules is ubiquitous in all aspects of life and material science, much is yet to be learned about their behavior, even at the most basic level. Among the many compounds that exhibit self-ordered structures, the polyphilic liquid crystals are of particular interest. This class of compounds is characterized by a dominant nonspherical rigid core and constituent moieties with some degree of energetic incompatibility.¹ The antagonistic nature of the molecular segments conduces the formation of periodic two and three-dimensional microsegregated structures. Apart from the now common exploitation of liquid crystals for their optical properties, polyphilic LC systems are of further interest from a biological perspective as potential biomimics or for drug delivery via encapsulation. Because of their inherently fluid nature, they have self-healing properties and, as such, constitute interesting engineering materials by themselves or in separation processes when used as membranes. Finally, their self-assembled architectures could conceivably be used as templates for mesoporous materials.^{2–4}

When considering polyphilic liquid crystal mixtures, the phase space to be explored increases dramatically from that of the pure

compound, allowing the possibility of encountering new phases or affecting the stability of existing ones. We focus in this report on the mixture behavior of a unique family of mesogenic molecules that share the same broad aspects: a rigid polyphenyl unit that is terminally substituted with self-associating groups and laterally substituted with a chemically incompatible chain. The rigid unit with associating end groups is in essence a bolaamphiphile;^{5,6} hence, these compounds are termed T-shaped bolaamphiphiles (TsB).

A recent review by Tschiesske showcases the synthesis and characterization of these compounds.⁷ The relative incompatibility between molecular components causes these compounds to have rich phase behavior, even as pure substances. Experimental analysis, through polarized light optical microscopy, differential scanning calorimetry, and X-ray scattering, have indicated at least 11 unique self-assembled liquid structures that form, depending on the length and chemical properties of the grafted chains. The phases observed are typically columnar phases, in which the lateral chains segregate into honeycombed cylinders of bolaamphiphilic rigid-unit networks, or lamellar phases composed of lateral chain-rich

Received: December 3, 2010

Revised: January 31, 2011

Published: March 18, 2011

and bolaamphiphilic unit-rich layers. The resulting geometry and stability of the microsegregated domains is a complicated function of the size of the different incompatible units. It is drawn from the experimental data that the formation of these mesostructures is not sensitive to the precise chemical nature of the side chain, as long as they have different interactions with the LC core of the parent molecule, and is apparently largely governed by the molecular volume fraction, f , of the side chain. Similarly, the position of the graft and detail of the polar end groups seems relatively unimportant.⁸ In fact, alternative molecular structures, such as facial amphiphiles, in which the self-associating groups are part of the lateral chain as opposed to being the rigid mesogen end groups, exhibit similar phase behavior.⁹

The nonspecific nature of the problem suggests that the study of generic self-assembly traits may be performed by means of molecular simulation of coarse-grained analogues. We have previously reported such studies for pure TsB's,¹⁰ the results of which were independently confirmed by the dissipative particle dynamics simulations of Bates and Walker.¹¹ In agreement with experimental results, a rich mesophase behavior has been seen. This approach has also been successful in studying the phase behavior of similar rigid–flexible block copolymers systems (see, e.g., refs 12–17).

The lyotropic behavior of polyphilic liquid crystal has received much less attention in the literature, most likely because of the very complex phase diagrams that may arise (see, for example, ref 18). There is, however, a unique report by Qi et al. on the effect of adding surface-coated gold nanoparticles to columnar assemblies of T-shaped bolaamphiphiles similar to those modeled here.¹⁹ The nanoparticles had been grafted with either hydrophobic (hexane thiolate) or hydrophilic (triethylene glycol-terminated pentane thiolate) monolayers. Qi et al. reported that the phase stability of the columnar phase critically depends on both the type and the concentration of the nanoparticles. The hydrophobic nanoparticles, which most likely concentrate on the column interior, showed a destabilizing effect on the phase structure. On the contrary, the hydrophilic nanoparticles had a stabilizing effect on the structure up to a weight concentration of approximately 10%. Furthermore, under certain conditions, there was evidence of distinct columnar phases and possibly different mesoscopic domains within the sample.

The present report systematically studies these issues, describing the effect of mixing TsB's with several solvents, which in turn are representative of the different segments of the polyphilic molecule.

2. MOLECULAR MODEL

All-atom simulation approaches to studying macromolecular self-assembly are hampered by both long time scales and minimum system size requirements. Both aspects conspire to request computational resources well beyond those available now and in the foreseeable future. Coarse-graining (CG) techniques allow, at least partially, the resolution of these issues. A full review of CG techniques for fluids and soft matter is beyond the scope of this paper, and the reader is referred to recent reviews on the topic.^{20,21} It suffices to say that most common techniques start with an atomistic description of a molecule, grouping elementary atoms and charges into “super-atoms”. Different methodologies exist to map the properties of these superatoms with the expected properties of the parent atomistic model. Nonexhaustive examples are to angle-average the pairwise potentials,²² to perform

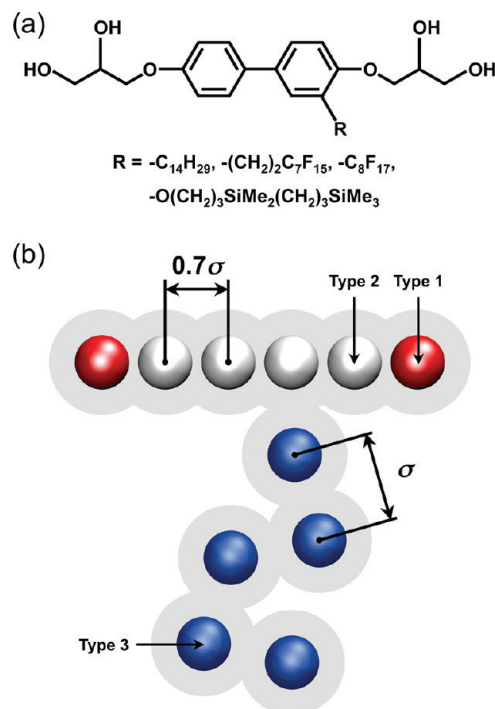


Figure 1. (a) A typical T-shaped polyphilic molecule that exhibits the Col_h phase. The core of the molecule is a rigid unit 4,4'-bis(2,3-dihydroxypropoxybiphenyl) with a grafted chain R, where R may be an alkane chain, $\text{C}_{14}\text{H}_{29}$ (compound 1/14 in ref 33); a semiperfluorinated chain, $(\text{CH}_2)_2\text{C}_7\text{F}_{15}$ (compound 2/i7 in ref 34); a perfluorinated chain, C_8F_{17} (compound 4/8 in ref 34); or a carbosilane group, $\text{O}(\text{CH}_2)_3\text{SiMe}_2(\text{CH}_2)_3\text{SiMe}_3$ (compound C4 in ref 35). (b) Schematic of molecular model used to describe T-shaped bolaamphiphiles. Type 1 beads are red, type 2 beads are white, and type 3 beads are blue.

matching to structural properties,²³ or to match the forces between groups of atoms.²⁴

In contrast, our approach to describing complex soft matter follows a route that has historically been successful in describing simple atomistic and molecular fluids. In this top-down approach, the structure of the fluid is described by a collection of spherical hard cores at densities that may be matched to experimental densities.^{25,26} Attractions between the fluid particles, resulting from dispersion interactions, electrostatics, and possible hydrogen bonding, are treated as perturbations, which are added sequentially. This approach has been the underlying proposition behind the development of modern equations of state, such as SAFT,^{27,28} which are able to link intermolecular potentials with macroscopic properties. Although not detailed here, a link can be made between the simple description of coarse-grained moieties and a macroscopic equation of state that may be used to obtain the average parameter sets. The resulting methodology leads to the description of transferable potentials; for example, superatoms that can be used as elements of group-contribution models. Successful coarse-grained force fields, such as the MARTINI²⁹ or Shinoda et al.³⁰ force fields, are also fundamentally based on the same premise of using simple building blocks.

Our coarse-grained model of a TsB has been outlined previously;¹⁰ however, for completeness, we briefly describe it again. To model the mesogenic core of the TsB, we use six interaction site beads held in a rigid linear arrangement. To describe the flexible lateral group, a chain of five beads attached to the third

Table 1. LJCS Parameters Used for Each Nonbonded Pair Potential, Parameters Listed As (ϵ_{AB} , σ_{AB} , C_{AB})

| | type 1 | type 2 | type 3 |
|--------|-----------------------------------|-----------------------------------|-----------------------------------|
| type 1 | $\epsilon, \sigma, 2\sigma$ | $\epsilon, \sigma, 2^{1/6}\sigma$ | $\epsilon, \sigma, 2^{1/6}\sigma$ |
| type 2 | $\epsilon, \sigma, 2^{1/6}\sigma$ | $\epsilon, \sigma, 2^{1/6}\sigma$ | $\epsilon, \sigma, 2^{1/6}\sigma$ |
| type 3 | $\epsilon, \sigma, 2^{1/6}\sigma$ | $\epsilon, \sigma, 2^{1/6}\sigma$ | $\epsilon/2, \sigma, 2\sigma$ |

bead of the rigid unit was used. The resultant topology of the molecular model is illustrated in Figure 1b. The ratio of lateral chain volume to total molecule volume, f , is around 0.44, commensurate with that of the target compound. The interbead separation within the rigid unit was chosen as 0.7σ , where σ is a characteristic model length, defined as roughly a bead diameter, giving the core an aspect ratio of approximately 4.5. To model the bonded interactions between flexible lateral chain beads and the bond of this chain to the rigid unit, a harmonic potential of the form

$$U^{\text{har}} = \frac{1}{2}k_{\text{sp}}(r - r_o)^2 \quad (1)$$

was used, where r is the bead separation, r_o is the equilibrium separation, and k_{sp} is the spring constant. In the model, an equilibrium distance of $r_o = \sigma$, and spring constant of $k_{\text{sp}} = 50(\epsilon/\sigma^2)$ were used. Here, the spring constant is a function of ϵ , a characteristic energy of the model, defined in terms of the interbead pair potential. Although the lateral chain has complete flexibility, it should be noted that each bead corresponds to a group of atoms; consequently, it is similar to coarse-grained models typically used for polymer systems.³¹

To mimic bolaamphiphilic behavior in the rigid-unit mesogenic core, both end beads were defined to attract each other in a preferential way, mimicking strongly interacting multiple hydrogen-bonding sites, whereas the remaining pair interactions were modeled as softly repulsive so as to allow the internal beads to represent weakly interacting sites typical of a polyphenyl core. The lateral chain beads are weakly self-attracting. Hence, the beads were categorized into three different types, here named type 1 for the rigid-unit end beads, type 2 for the rigid-unit interior beads, and type 3 for the flexible lateral chain beads. These are schematically colored coded in Figure 1b. For simplicity, all six bead pair potentials were defined through the Lennard-Jones (LJ) cut and shifted potential, U_{AB}^{LJCS} , given by

$$U_{AB}^{\text{LJCS}}(r; C_{ij}) = \begin{cases} U_{AB}^{\text{LJ}}(r) - U_{AB}^{\text{LJ}}(C_{AB}) & \text{for } r < C_{AB} \\ 0 & \text{for } r \geq C_{AB} \end{cases} \quad (2)$$

with

$$U_{AB}^{\text{LJ}}(r) = 4\epsilon_{AB} \left[\left(\frac{\sigma_{AB}}{r} \right)^{12} - \left(\frac{\sigma_{AB}}{r} \right)^6 \right] \quad (3)$$

where the subscripts A and B define bead type, r is the bead separation, ϵ_{AB} is an energy parameter defining the potential well depth, σ_{AB} is a length parameter that defines the potentials range, and C_{AB} is the cut and shift distance. The parameters used for each pair potential are summarized in Table 1. In this parametrization, all bead pairwise interactions have the same σ_{AB} , set equal to σ . The C_{AB} of $\sigma_{AB}^{1/6}$ is used for all cross-interactions. Type 2 bead self-interactions correspond to a cut and shift at the

Table 2. (a) Experimental and Model Phase Transition Temperatures of the $N_{\text{flx}} = 0$ Nongrafted Bolaamphiphile^a and (b) Phase Transition Temperatures for the Model $N_{\text{flx}} = 5$ T-Shaped Bolaamphiphile As Compared with Experimental Analogues^b

| data source | (a) | | ref |
|--|--|---------------------------|--------------------|
| | R | phase transition T (°C) | |
| experimental | Cr 245 SmA 294 Iso | | 33 |
| simulation | Cr 171 SmA 294 Iso | | |
| (b) | | | |
| R | phase transition T (°C) | f_{side} | ref |
| (CH ₂) ₃ C ₇ F ₁₅ | Cr 56 Col _h 171 Iso | 0.46 | 2/i7 ³⁴ |
| C ₁₄ H ₂₉ | Cr 100 Col _h 142 Iso | | 1/14 ³³ |
| O(CH ₂) ₃ SiMe ₂ (CH ₂) ₃ SiMe ₃ | Cr 70 Col _h 117 Iso | 0.46 | C4 ³⁵ |
| C ₈ F ₁₇ | Cr 97 U 134 Col _h 158 Iso | 0.43 | 4/8 ³⁴ |
| this work ($N_{\text{flx}} = 5$) | Cr 31 CrII 64 Col _h 216 Iso | 0.44 | |

^a Model data is scaled using $\epsilon/k = 567$ K to match the experimental smectic A–isotropic transition. ^b Compare with Figure 1a. Model data is scaled using $\epsilon/k = 567$ K. Here, f refers to the volume fraction of the lateral chain to that of the whole molecule. Phases: Cr and CrII, crystalline; U, unknown; Col_h, hexagonal columnar; Iso, isotropic; SmA, smectic A.

minimum of the LJ potential, thus map into a soft-repulsive WCA fluid.³²

To explore mixture phase behavior of TsB and solvent binary mixtures, the model is extended to include solvents. Retaining the minimalist approach of the original model, we chose to investigate three solvent types, each modeled as single nonbonded beads equivalent to each of the three bead types found in the TsB molecule; that is, we considered three solvents, each constituted by a fluid of unbound spheres, characterized by pair potentials of the form specified in eqs 2 and 3.

3. SCALING TO REAL UNITS

Implicitly, we have taken as a case study the grafted 4,4'-bis(2,3-dihydroxypropoxy-biphenyl) molecule. With an appropriate side chain, this molecule self-assembles into 2D hexagonal columnar structures (Col_h). Examples of such side chains could be an alkane chain, C₁₄H₂₉ (compound 1/14 in ref³³); a branched semiperfluorinated chain, (CH₂)₃C₇F₁₅ (compound 2/i7 in ref³⁴); a perfluorinated chain, C₈F₁₇ (compound 4/8 in ref³⁴); and even a carbosilane group, O(CH₂)₃SiMe₂(CH₂)₃SiMe₃ (compound C4 in ref³⁵). We note that these are neither the only compounds that produce these Col_h structures nor the only TsB's that could be represented.

We have not attempted to fit our molecular model to any particular substance; however, one is tempted to compare the phase transition temperature observed from the simulations to those from experiments. Table 2a and b presents such a comparison both for the core LC model (without lateral chain) and for several examples of T-shaped bolaamphiphiles. The bolaamphiphilic core exhibits only an LC smectic A phase both in the experiments and in the model. At this point, one could match the smectic–isotropic phase transition temperature of the pure nongrafted bolaamphiphile with that used in the molecular model and thus obtain the model's single energetic scale as $\epsilon/k = 567$ K. Clearly, other phase transition temperatures or averages could

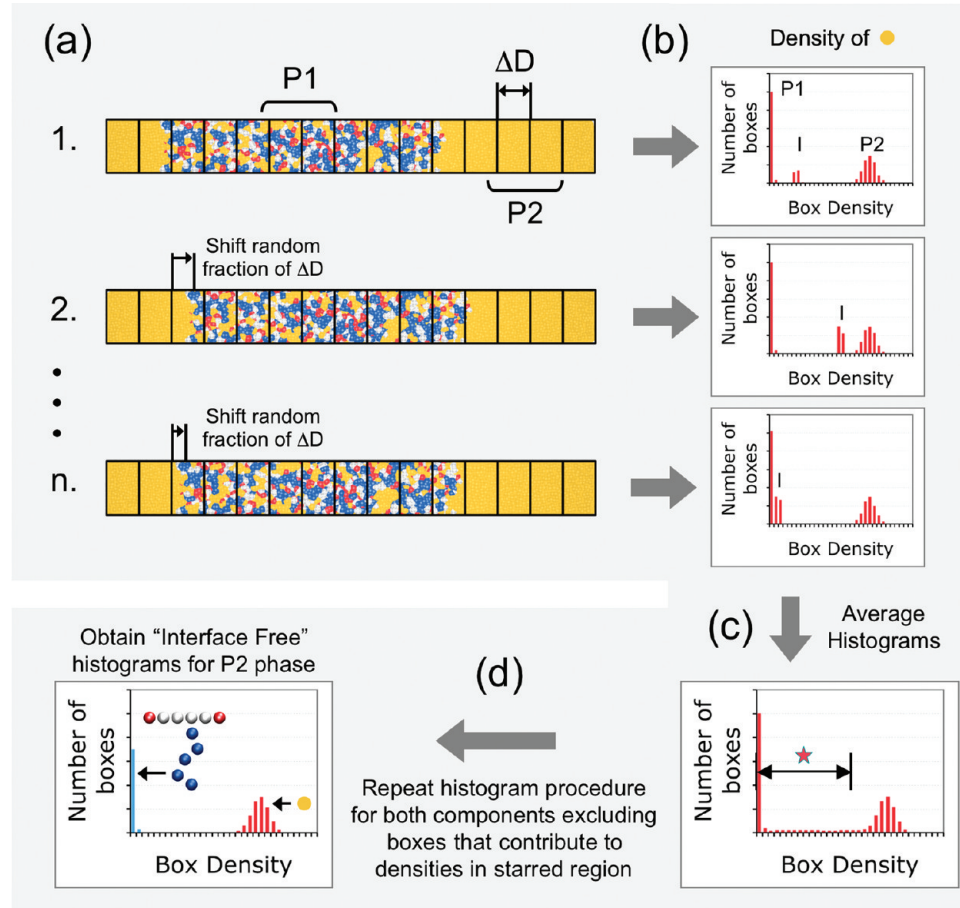


Figure 2. Diagram outlining the density profiling method. By displacing the lattice used to generate histograms through random fractional displacements, many lower-quality histograms may be produced. Averaging over these histograms produces an improved quality histogram, amenable for using to select boxes of one phase; i.e., discounting boxes that include the interface (I). The histogram-averaging procedure is then repeated with the selected single-phase boxes, either P1 or P2 boxes, generating histograms for both components in this phase. The method can then be repeated for the other phase.

have been taken if required, notwithstanding, this comparison is made to exemplify the generic nature of the self-assembly process. Despite this crude scaling, Table 2b shows how the phase transition temperatures compare quantitatively between the model and experimental data for diverse real molecules.

The general nature of the strong and multiple attractions experienced by type I molecules suggest that it would correspond to a polar, hydrophilic solvent with a capability of multiple self- and cross-hydrogen bonding. If the energy parameter in our model is mapped to $\varepsilon_{11}/k_b = 567$ K (c.f., Table 3a), a type 1 bead will correspond to a fluid with a critical temperature of approximately the same numerical value, since the reduced critical temperature of a shifted LJ fluid is close to unity,³⁶ thus suggesting a solvent similar to propanol.

In a similar spirit, and by inspection of the originating molecule (Figure 1a), a type 2 bead may be associated with aromatic-like solvents, such as benzene or toluene. Note that although in the LC backbone, four type 2 beads represent a biphenyl group, we have chosen to fuse the model beads to impart rigidity to the backbone of the model; hence, these fused type 2 beads occupy not much more volume than two tangent spheres of the same diameter.

The type 3 bead solvent represents a fluid compatible with the side chain moiety. If one considers the side chain to be a perfluorinated chain, from Table 2b, it can be observed that a

five-bead chain would map into a perfluoroctane. The closest sterical mapping suggests that each type 3 bead corresponds roughly to a perfluoroethane molecule. The critical temperature of perfluoroethane ($T = 293$ K) agrees qualitatively with that expected from a cut and shifted LJ fluid of well depth $\varepsilon_{33}/k_b = 281$ K. Considering the critical density of the cut and shifted LJ fluid³⁶ and that of the proposed model fluids, one may estimate the size parameter to be close to $\sigma = 0.5$ nm, consistent with the expected dimensions of the model fluid and solvents. The bead mass may also be estimated from these rough guidelines. A propanol bead would have a molar mass of 60 g/mol; a benzene bead, 78.1 g/mol; and a perfluoroethane bead, 138 g/mol. In our model, all beads are considered to be of identical mass, which crudely would map into beads of molecular mass 100 g/mol. This last result affects only the translation of time steps and eventually of diffusion, which is not discussed herein. Each simulation time step may be related to reduced time by the formula, $t^* = t/(m\sigma^2/\varepsilon)^{1/2}$, with m defined as the bead mass. From the above discussion, in our simulations, $(m\sigma^2/\varepsilon)^{1/2}$ took a value of 2.31 ps.

Despite the self-consistency of the model parameters used and their clear relation to experimentally observed properties, we chose here to describe the fluid behavior in terms of generic reduced parameters, rather than the experimental scales, to reinforce the point that we have not attempted to model an exclusive solute/solvent system, but rather, to explore generic behavior. As a

consequence, we present all properties in a reduced form in terms of single length, σ , and energy, ε , scale. Here, temperature is given by $T^* = Tk_b/\varepsilon$, where k_b is Boltzmann's constant, pressure is given by $P^* = P\sigma^3/\varepsilon$, and number density is given by $\rho^* = N\sigma^3/V$, where V is the total volume and N may refer to a molecule or a bead, depending on the context.

4. PHASE CHARACTERIZATION

The structured phases observed during simulations were monitored through computation of order parameters and density distributions from output configuration data. These allowed a quantitative understanding of the phases to be achieved and helped locate phase transitions. An important requirement for many of these metrics was the need to assign a director axis to the phase structure. A natural director associated with the hexagonal columnar phase is the columnar axis itself. We chose to approximate this with the unit vector orientated maximally orthogonal to the set of vectors pointing along each TsB rigid unit. A more detailed outline of this is given elsewhere.¹⁰ The set of metrics based on this director, as well as a density distribution metric, are discussed in more detail in the following subsections.

4.1. Order Parameters. To determine the degree of columnar order, we defined the planar order parameter, S_2 , to measure the level of orthogonality between the molecular orientation vectors and the director vector via the equation

$$S_2 = \frac{\sum_{j=1}^N 3 \sin^2 \phi_j - 1}{2N} \quad (4)$$

where ϕ_j is the angle between the director and the orientation vector of the j th molecular rigid unit. This order parameter is similar to the P_2 order parameter used to study orientation order of calamitic mesogen systems.³⁷ For an isotropic system, the director and orientation vectors are uncorrelated, and S_2 by definition takes a value of 0. Conversely, for ordered systems in which all molecular orientation vectors are orthogonal to the director, S_2 takes a value of 1. The order parameter monotonically increases with increasing system order between these extremes.

To monitor columnar phase, two-dimensional geometric order, as seen from an observer looking into the director, we used the planar orientational order parameter, ψ_k , defined through the equation

$$\psi_k = \left| \frac{1}{N} \sum_{j=1}^N \exp(ik\theta_j) \right| \quad (5)$$

where θ_j is the angle between the vector given by the projection of the j th TsB rigid unit vector onto the director orthogonal plane and a fixed arbitrary axis orthogonal to the director. The coefficient k takes the value 2, 3, 4, and 6 for the linear, triangular, square, and hexagonal planar orientational order parameters, respectively. As with the planar order parameter, by definition, it monotonically increases from 0 to 1 on going from the unordered to fully ordered state.

4.2. Director Orthogonal Density Profiles and Columnar Swelling. To explore solvent localization in the columnar structures as well as columnar swelling, it proved useful to investigate bead density profiles across planes orthogonal to the column. Bead densities were obtained by projecting the positions of each bead in the simulation box onto an arbitrary plane

orthogonal to the column director. By discretizing this plane into small bins and counting the number of particles in each grid box, an uncorrected density was obtained. Since a different volume of simulation box is projected through for each grid box, the particle counts are divided by this volume to obtain corrected densities. To avoid the complication of analytically calculating these volumes, a Monte Carlo procedure was used to find accurate estimates of these.

During the density distribution analysis, it was straightforward to obtain the simulation box's projected area on the director orthogonal plane. Since in regions of stable structured phases, the number of columns in the simulation box remained constant over state points, direct comparison of these projection areas permitted a quantitative analysis of columnar swelling between state points.

4.3. Molecular Density Distribution. Molecule density distributions were useful for many aspects of our investigation into the mixture phase behavior (in particular, to follow phase separations from initial nonequilibrium homogeneous states) and for determining bulk densities of coexisting phases in biphasic simulations.

To determine the density distribution of a given configuration, the simulation box was divided into congruent volumes of shape similar to the simulation box, the number of solvent particles found in each box was counted, and a histogram of densities was produced. Since this distribution is dependent on the relative position of the phase interface with respect to the simulation boxes' dividing lattice, the lattice was displaced through the simulation box by random amounts, taking into account the periodic boundaries, and density histograms were constructed for each and then averaged. The output of this method produced histograms that include contributions from interfacial regions of the simulation box. As the MD cell volume changes during constant pressure ensemble simulations over timesteps, so too does the set of discrete densities output from such an analysis. A linear interpolation was used to map these changing discrete densities onto a fixed density grid, permitting averaging of histograms over multiple timesteps.

Although these distributions, containing an interfacial contribution, were suitable for monitoring phase separation, they were not appropriate for obtaining bulk densities, since this involves performing integrals over the distribution peaks. To overcome this problem, it was necessary to have some criteria to assign different regions of the simulation box to one of the bulk phases or to the interfacial regions.^{38,39} An outline of the novel method implemented is given in Figure 2. As seen in Figure 2b, the contribution of interface-containing boxes to the component's histograms are lattice-displacement-dependent. This property was used to pick out such regions. To that end, a component was initially selected, and the position of its highest density distribution peak, corresponding to its rich phase, was determined. As seen in Figure 2c, by setting a threshold level below this peak, it proved possible to identify lattice boxes containing interface regions when a lattice displacement led to their peaks lying at comparatively low densities (c.f. the top histogram of Figure 2b). Such a criterion also automatically identifies boxes containing the selected component's dilute phase. Consequently, by performing the histogram procedure for both components, excluding these identified boxes, the density profiles for each component in the selected component's rich phase were generated, as shown in Figure 2d. The procedure was then repeated, but selecting the other component and, hence, providing density data on the other

coexisting phase. The criterion used for discounting boxes was to neglect the ones with densities below the identified densest peak's position less 0.6 of its width.

5. PURE FLUID BEHAVIOR

Before describing the results for the mixture of TsB and solvents, we briefly review some highlights of the phase behavior for TsB molecules of varying lateral chain length.¹⁰ Here, three distinct phase structural classes are found. For the system without lateral chains, LC phases typical of rodlike mesogens are formed. The introduction of a lateral chain increases hindrance to rigid-unit alignment and results in columnar phase formation at intermediate chain lengths. Finally, for molecules with relatively large side chains, the columnar structure becomes unfeasible, and lamellar phases form. In the following section, a summary of the pure component phase behavior is given for the representative models with $N_{\text{flx}} = 0$ and $N_{\text{flx}} = 5$, where N_{flx} refers to the number of beads in the side chain.

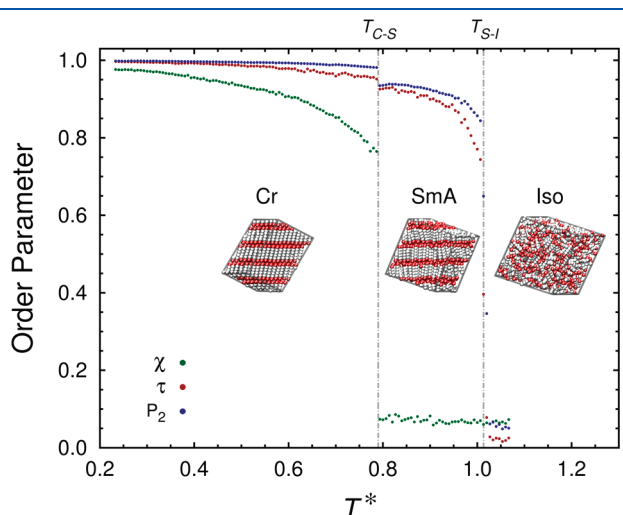


Figure 3. Phase diagram displaying the crystalline, smectic A and isotropic phases observed for the underlying pure bolaamphiphilic rod model with no lateral flexible chain ($N_{\text{flx}} = 0$). Visual inspection accompanied by an analysis of the hexagonal order parameter, χ ; the layering order parameter, τ ; and the nematic order parameter, P_2 , were used to differentiate the phases. Vertical lines denote the phase transition temperatures from crystal to smectic A (T_{C-S}) and from smectic A to isotropic (T_{S-I}). Simulations were performed at $P^* = 0.63$.

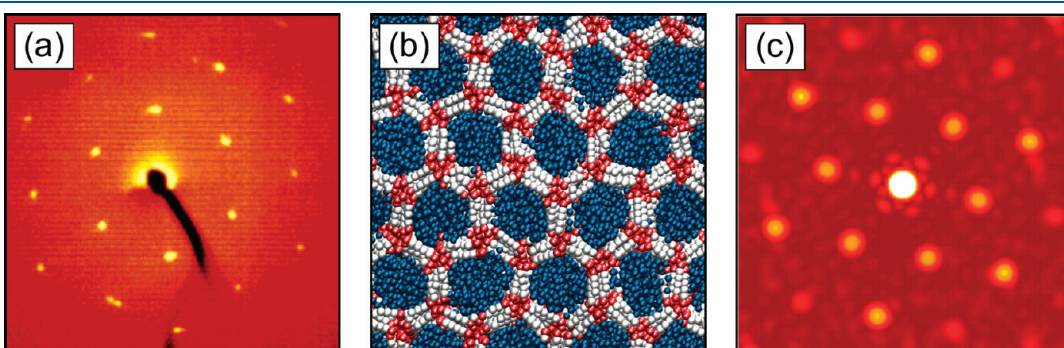


Figure 4. (a) X-ray diffraction pattern of hexagonal columnar mesophase with alignment of columns on a glass substrate (compound 2/i7 at 175 °C of ref 34) (reprinted with permission from ref 34, copyright 2003 American Chemical Society). (b) A snapshot of the hexagonal columns formed during an MD simulations of a pure $N_{\text{flx}} = 5$ TsB, $T^* = 0.67$, and $P^* = 0.78$. (c) Calculated X-ray pattern of the configuration in panel b using bead densities orthogonal to the columnar axis.

5.1. Calamitic Bolaamphiphile $N_{\text{flx}} = 0$. The reference TsB without lateral chain is, in effect, a calamitic bolaamphiphilic mesogen. The pure bolaamphiphile system was studied in a temperature range of $T^* = 0.13 - 1.06$ and at $P^* = 0.63$. Further simulation details are included in section 1 of the Supporting Information. To survey phase stability regions, three commonly used order parameters for prolate mesogen studies were calculated. A hexagonal order parameter, χ , was used to ascertain inlayer hexagonal close packing of orientationally ordered and layered rod molecules, distinguishing crystalline phases from the smectic A phase, that is, characterized by inlayer diffusion. A layer order parameter, τ , which quantifies molecular layering order, provided a distinction between the smectic A and nematic/isotropic phases. Finally, an orientational order parameter, P_2 , to study orientational order allowed a distinction between nematic and isotropic phases. As standard, all these order parameters are defined to monotonically pass from 0 to 1 with increasing system order. Further order parameter details are included in section 1 of the Supporting Information.

The results of the pure phase $N_{\text{flx}} = 0$ order parameter analysis are summarized in Figure 3. Below $T^* = 0.8$, all order parameters

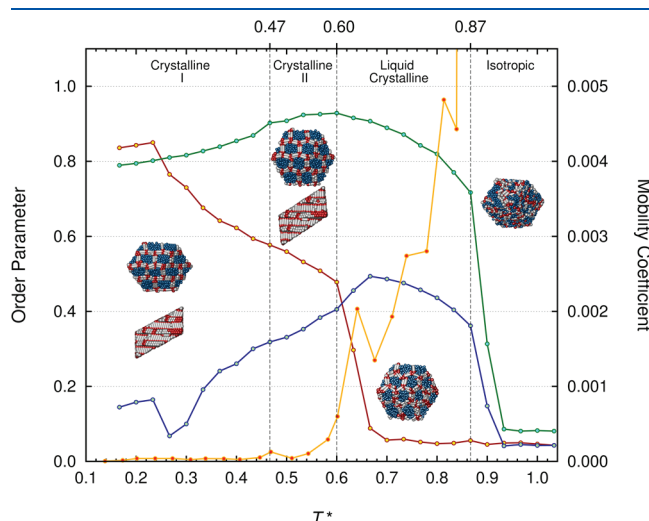


Figure 5. Order parameters (left ordinate) and mobility coefficient (right ordinate) for the pure $N_{\text{flx}} = 5$ TsB as a function of temperature. Green line is the planar order parameter, S_2 ; maroon line is the square columnar order parameter, ψ_4 ; blue line is the hexagonal columnar order parameter, ψ_6 ; and yellow line is the mobility coefficient. Vertical lines denote the phase boundaries. Simulations were performed at $P^* = 0.78$.¹⁰

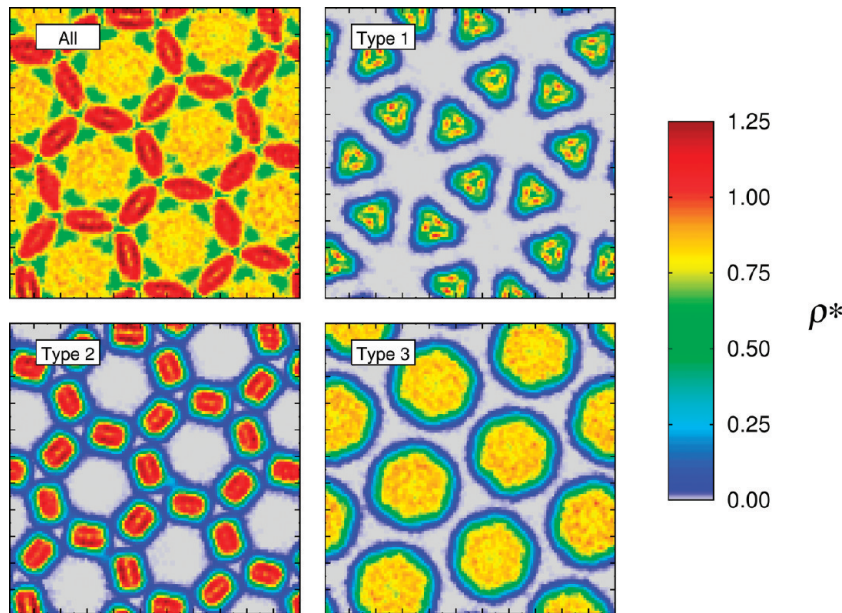


Figure 6. Director orthogonal density, ρ^* , profiles for all particle types (equivalent to global density) and for each of the particle types, taken from an MD simulation of a pure $N_{\text{fix}} = 5$ TsB system that forms hexagonal columnar LC phase. The simulation was performed at $T^* = 0.67$ and $P^* = 0.78$.

are close to 1, indicating fully crystalline structures, an illustrative snapshot of which is shown in the diagram. On increasing the temperature above $T^* = 0.8$, a drop in χ is observed, indicating inlayer diffusion of the rod molecules and, hence, the appearance of a smectic A phase. Finally, above $T^* = 1.0$, there is a drop in both τ and P_2 , indicating a transition from the smectic A directly to the isotropic phase. In a separate study, not included herein, into a related longer aspect ratio bolaamphiphilic mesogen, the nematic phase was observed as stable only at higher temperatures and pressures. The effect of increasing terminal bead self-attractions was also found to destabilize the nematic phase at lower temperatures and pressures. Consequently the lack of nematic phase here may be attributed to the high energetic penalty of breaking the layering dominating over the entropic favorability of the smectic A to nematic transition.

5.2. Columnar Phases: $N_{\text{fix}} = 5$ T-Shaped Bolaamphiphile.

By attaching lateral chains to the rigid LC core, one stabilizes columnar mesogenic phases, passing from triangular columnar, through to square columnar and, finally, hexagonal columnar, with increasing lateral chain length.^{10,11} Here, we focus on the $N_{\text{fix}} = 5$ structure that forms stable hexagonal columnar structures, an example of which is given in the simulation snapshot of Figure 4b. As with other model systems, the phase behavior was investigated over a range of temperatures at constant pressure of $P^* = 0.78$, using order parameters and mobility coefficients to differentiate phases. The results are summarized in Figure 5. Upon cooling from high to low temperature, the change from an isotropic to hexagonal columnar phase is shown by a jump from near zero values of S_2 and ψ_6 to values of around 0.72 and 0.36, respectively, at $T^* = 0.87$. With a further temperature decrease, both S_2 and ψ_6 slowly increase until $T^* = 0.50$, where there is a jump in ψ_4 . Below this temperature, ψ_4 increases while S_2 and ψ_6 slowly decrease.

The nonzero values of mobility coefficient (that is, related to the mean square displacement of TsB molecules) in the range $T^* = 0.50–0.87$, in addition to an observed self-assembly from an isotropic configuration to the structured phase in an MD

simulation at $T^* = 0.73$, suggest this phase is liquid crystalline. It is this phase which we use as a reference for most of the mixture studies reported herein. The underlying distribution of angles of which ψ_6 is a function is also relatively slow-varying, which accounts for the intermediate values of ψ_6 . This suggests some molecular movement around the column interior and further supports the previous phase characterization. In Figure 4, both an X-ray pattern obtained from a real hexagonal columnar-phase-forming molecule, along with a calculated X-ray diffraction pattern from the simulation bead densities, are presented. The qualitative similarities of these patterns demonstrate the agreement between the experimental phase structure and that of our simulated model. Finally, the director orthogonal density of the pure TsB liquid crystalline phase is presented in Figure 6. As will be shown, this was useful as a reference when studying low-solvent-concentration TsB mixtures.

6. SIMULATION DETAILS

All simulations were performed in continuum space via molecular dynamics with the DL_POLY simulation suite.⁴⁰ The extended-Lagrangian approach was used to simulate either the constant stress-isothermal $N\sigma T$ ensemble or the isobaric-isothermal NPT ensemble, the former being implemented for simulations containing nonisotropic phases (the predominant case for our studies). All simulations were performed with a time step of $\Delta t^* = 0.0125$ and with periodic boundary conditions. Further details of the chosen barostat and thermostat relaxation constants are given in section 2 of the Supporting Information.

To explore different aspects of the $N_{\text{fix}} = 5$ TsB and solvent phase behavior, three unique series of molecular dynamic simulations were performed. The first involved studying solvent effects on the hexagonal columnar structure in the low solvent composition limit focusing on columnar swelling and solvent positioning. The second series of simulations were performed across the full composition range, aiming to identify possible phase coexistence or transitions into other mesogenic phases.

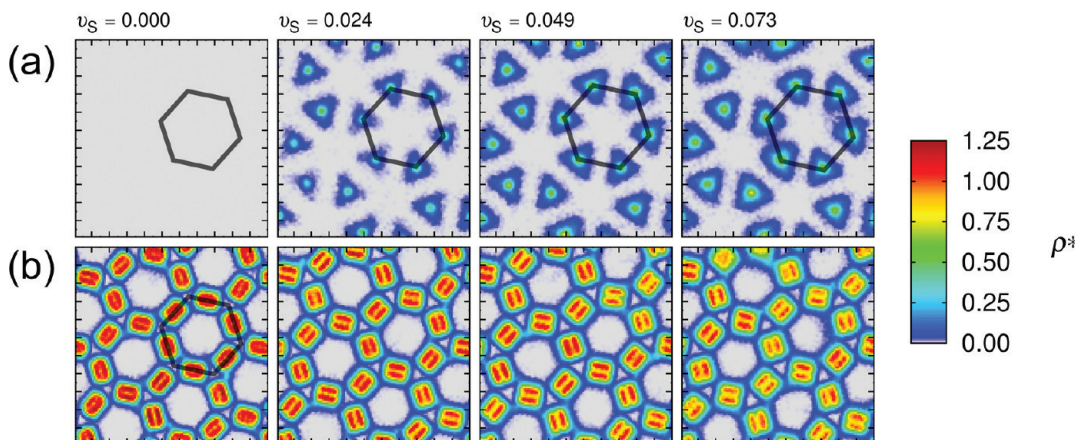


Figure 7. Director orthogonal density profiles, ρ^* , for the TsB and type 1 bead solvent mixture at low solvent concentration: (a) type 1 solvent beads and (b) type 2 TsB rigid-unit beads. The black line hexagons describe the positioning of the TsB rigid-rod units in the hexagonal columnar structures and are shown for reference only. Simulations were performed at $T^* = 0.67$ and $P^* = 0.78$.

A third set of simulation runs were oriented toward simulation of coexistence of TsB-rich phases with solvent-rich phases over a range of temperatures.

In addition to this, a number of temperature-quench type simulations^{38,39} were performed from initial configurations of homogeneous and isotropic mixtures. The procedure allowed phase separation and self-assembly mechanisms to be dynamically observed. These simulations were an independent check of the stability of observed phase separations generated from other routes.

6.1. Composition Variation Simulations. For the first two series mentioned above, simulations were performed at $T^* = 0.67$ and $P^* = 0.78$, corresponding to a state point in the liquid crystalline range for the pure $N_{\text{fix}} = 5$ system. To efficiently study the effect of composition for an exhaustive range of state points, an identity exchange procedure was implemented. This involved converting the constituent beads of a random fraction of TsB molecules from an equilibrated configuration to solvent beads to produce a new configuration with a different composition that could be used as a nonequilibrated input for the next MD run. With this procedure, a systematic approach to alter solvent fraction while retaining total particle numbers was achieved, effectively modeling a sequential conversion process. Because these initial configurations were far from equilibrium, a two-step relaxation procedure was employed. In the first stage, the maximum force exerted on all beads was capped, thus limiting their accelerations, and allowing slow reorganization of the solvent from the energetically unfavorable initial configuration. The second equilibration stage, without force capping, allowed the system to relax into a stable phase. All system compositions are reported as the fraction of the total beads that are solvent, v_S .

For the low solvent fractions, simulations were performed using the sequential conversion method, initiated from a pure system of 4096 TsB molecules equilibrated in a LC hexagonal columnar phase. Each mixture point considered was simulated with an equilibration period of 200 000 steps, followed by a data collection period of 100 000 steps. The force on each bead was capped for the first 1000 steps. Configuration data was sampled every 1000 steps. Between simulations, the identities of 50 random TsB molecules were converted to solvent corresponding to increments of $\Delta v_S = 1.2 \times 10^{-2}$. The resulting nonequilibrated state was used as a starting configuration for the next simulation

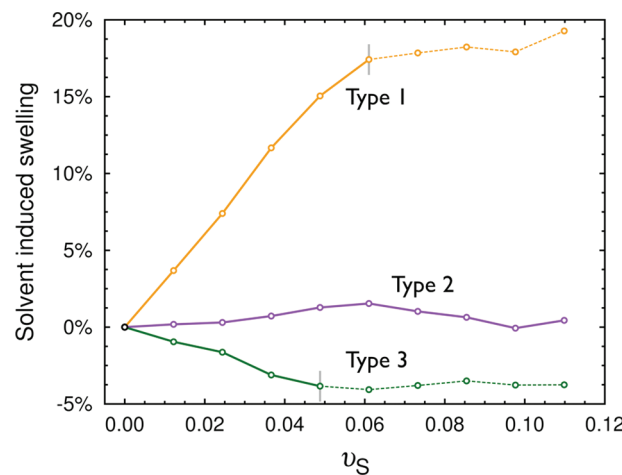


Figure 8. Diagram displaying the relative hexagonal column cross-sectional area for mixtures of solvent and TsB at low v_S , $T^* = 0.67$ and $P^* = 0.78$. The reference area is the cross-sectional area of the pure $N_{\text{fix}} = 5$ TsB system at the same T and P . The results for mixtures with type 1 bead (yellow line), type 2 bead (purple line), and type 3 bead (green line) are displayed. Also indicated is the hexagonal columnar cross-sectional area for the phase-separated type 1 solvent system (yellow dotted line) and the single-phase type 3 solvent system with partial hexagonal order (green dotted line).

in the series. Simulations were performed until reaching solvent compositions at which a phase separation or transition from the hexagonal columnar phase occurred.

For the full solvent composition series, a similar approach was used; however, simulations were initiated from a smaller pure system of 2000 TsB molecules. Due to an expected increased variation in phase structures between successive simulations, a longer equilibration of 300 000 steps, data collection of 500 000 steps, and sampling interval of 5000 steps was employed. The identity of 50 TsB molecules was switched between simulations, giving increments of $\Delta v_S = 2.5 \times 10^{-2}$, effectively modeling the full composition range from pure TsB to pure solvent by discrete steps.

6.2. Temperature Scan Coexistence Simulations. Guided by the composition variation simulation results described above, coexistence simulations were undertaken for type 1 and type 2

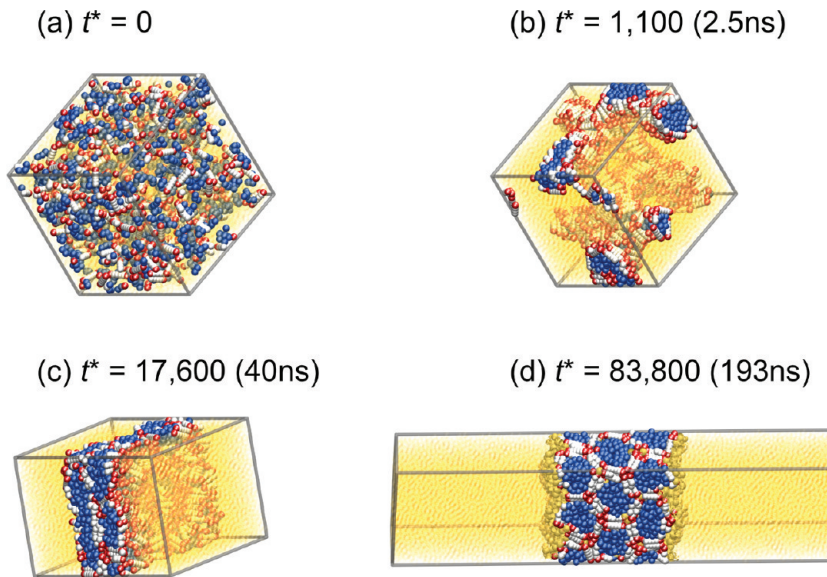


Figure 9. Diagram displaying the rapid phase separation, followed by self-assembly of an isotropic and homogeneous TsB and type 1 solvent mixture of overall $v_S = 0.750$. The type 1 solvent is indicated by yellow beads. Here, t^* corresponds to the reduced time, and numbers in parentheses correspond to actual time scaled according to the choice of energy, size, and mass parameters. Due to the coarse graining, real time is expected to be at least an order of magnitude larger. The simulation was performed at $T^* = 0.67$ and $P^* = 0.78$.

bead solvent mixtures. For both, systems of 2000 TsB molecules and 22 000 solvent beads, corresponding to $v_S = 0.5$, were initially equilibrated into configurations with coexisting mesogenic, hexagonal columnar TsB-rich phase and solvent-rich phases, at $T^* = 0.60$ and $P^* = 0.78$. Simulations were then performed over a temperature range using the output configuration of one simulation temperature as the input configuration for the next simulation temperature, from a lower bound temperature that exhibited crystalline–isotropic phase coexistence to an upper bound temperature characterized by complete miscibility. Temperature increments of $\Delta T^* = 1.7 \times 10^{-2}$ were used between simulations. For each simulation, an equilibration run of 400 000 steps was carried out, followed by data collection over 2 500 000 steps, with configurations sampled at 10 000 step intervals. Density analysis of output configurations was performed to ascertain TsB bead and solvent bead densities in each phase and, consequently, the v_S of each phase.

7. RESULTS

7.1. Type 1 Bead Solvent. *7.1.1. Low Solvent Fraction.* The results in the low solvent fraction region for the type 1 bead solvents are summarized by the director orthogonal density distributions given in Figure 7. Unsurprisingly, at low v_S , solvent beads are found to congregate in the hexagonal columnar vertices, where the possibility of multiple interactions with TsB type 1 beads favors their location. An illustrative snapshot of this effect from a $v_S = 0.037$ simulation is shown in Figure 1 of the Supporting Information. The outcome of this localization is to increase the columnar cross-sectional area, as channels of type 1 solvent form in the vertices and expand them relative to the solvent free conditions. Results of a columnar swelling study, obtained via the orthogonal density analysis, are presented in Figure 8. A linear increase in columnar area is seen for increasing v_S , up to $v_S = 0.060$. In this range of concentration, variation of solvent composition permits control over the phase structural dimension. Above $v_S = 0.060$, a

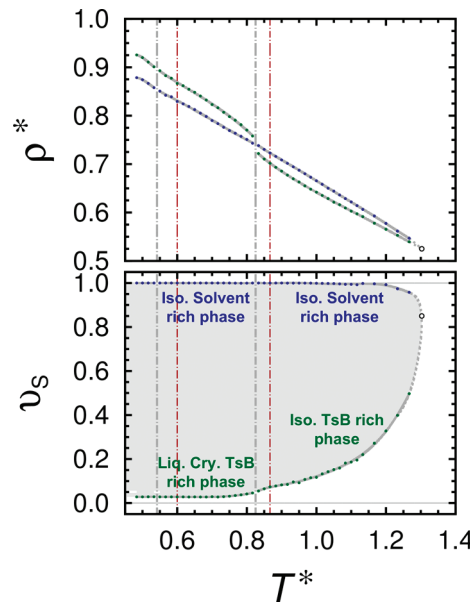


Figure 10. Plots of the phase densities, ρ^* , and phase solvent fractions, v_S , obtained by density analysis of biphasic MD simulations of a type 1 bead solvent and TsB mixtures. Gray vertical lines show the minimum and maximum temperature for which the columnar LC structure is present in one of the coexisting phases. Red vertical lines mark the minimum and maximum temperatures for which the pure $N_{\text{flx}} = 5$ TsB system exhibits columnar liquid crystalline behavior (c.f. Figure 5). Simulations at $T^* > 1.13$ were performed at overall $v_S = 0.7$, with equilibrations of 500 000 steps and data collections of 7 000 000 steps. Simulations were performed at $P^* = 0.78$.

relative saturation of the structure is achieved and the energetic cost of increasing the columnar interior area and, consequently, reducing TsB type 3 bead bonding presumably forces the system to phase-separate.

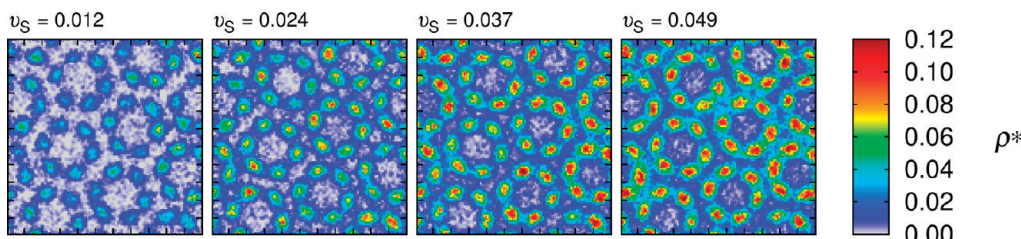


Figure 11. Director orthogonal density, ρ^* , and profiles of type 2 solvent beads in low solvent concentration mixtures at $T^* = 0.67$ and $P^* = 0.78$.

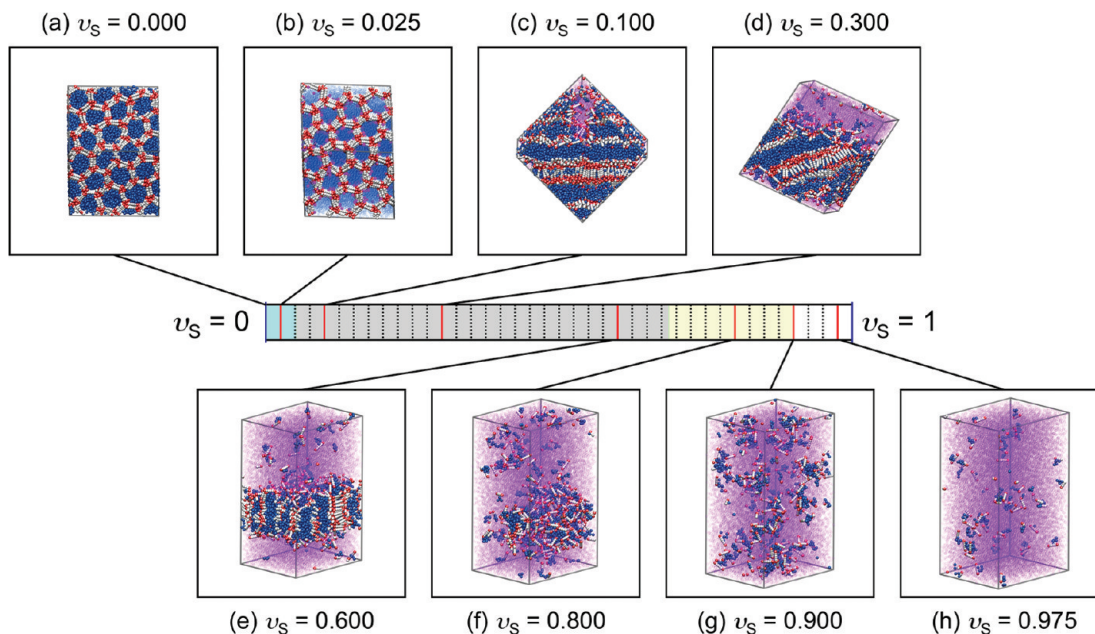


Figure 12. Snapshots taken from MD simulations at various type 2 bead solvent compositions, v_S . Type 2 solvent is indicated with purple beads. Different colors in the concentration graphic delineate the observed stages of mesophase segregation described in the main text. The simulation was performed at $T^* = 0.67$ and $P^* = 0.78$.

7.1.2. Full Composition Range. On increasing v_S across the full range of compositions, simulation configurations were generally found with a phase-separated, bolaamphiphile-rich, hexagonal columnar region and corresponding equilibrium solvent-rich regions. Despite the hexagonal columnar region's taking a distorted arrangement at lower solvent compositions, analysis of the phase's composition revealed it to be near the highest stable columnar phase composition observed during low solvent composition simulations. These structures were therefore concluded as being evidence not of a new mesophase, but most likely of metastable states. Further details of this analysis are given in section 4 of the Supporting Information.

To ensure the phase-separated configurations were not an artifact of the system being led through a series of metastable states during sequential conversion, a simulation initiated from a homogeneous and isotropic mixture at $v_S = 0.750$ was performed. Representative snapshots from different times during this simulation are presented in Figure 9. Here, a rapid separation of components occurred, initially creating a TsB micellar-like network structure, with TsB rigid units exposed to pure solvent and TsB flexible lateral chains enclosed in the micellar interior, as shown in Figure 9b. The network structure then rapidly coalesced into a distorted hexagonal columnar structure, as in Figure 9c, that itself on a much longer time scale relaxed to a

nondistorted structure, as in Figure 9d. This self-assembly into a state almost equivalent to that achieved via sequential conversion, though not affirming them as equilibrium states, is strongly suggestive. The times annotated in Figure 9 and the conversion to real units confer only an idea of the relative time scales for these processes. It is well understood that these CG “times” are orders of magnitude “faster” than the experimentally observed times.⁴¹

During the simulation, the initial rapid reorganization of TsB molecules, to expose only rigid-unit sections to the solvent phase, hints at a high interfacial tension in these biphasic simulations. This was born out by simulations at other v_S 's initiated correspondingly. Here, on some occasions, the simulation box distorted so significantly to minimize interfacial surface area that the simulations ended prematurely due to a box dimension being commensurate with the interparticle cutoff distance. During all biphasic simulations, edge of the columnar structures formed the TsB-rich phase interface with the solvent. This arrangement is energetically favorable compared with a solvent-exposed column-and-type interface. Here, only type 1 and 2 TsB beads are solvent-exposed, permitting solvent with TsB type 1 bead bonding while not disrupting columnar interior type 3 bead bonding.

7.1.3. Biphasic Simulations. Biphasic simulations over a range of temperatures were performed on the type 1 solvent mixtures

for a fixed overall v_S . Coexisting phase densities, ρ^* , and solvent compositions, v_S , obtained from density analysis are presented in Figure 10. For the saturated TsB-rich phase, discontinuities in densities and composition as well as inspection of simulation movies were used to locate phase transitions. Here, at $P^* = 0.78$, a transition is seen in the TsB-rich phase from a solvent-saturated crystalline phase to a saturated mesogenic phase, at $T^* = 0.54$ (c.f. $T^* = 0.60$ crystalline II-liquid crystal transition of Figure 5). In the resulting two phase system, upon heating, a transition is seen from the TsB-rich mesogenic phase to a solvent-saturated isotropic phase, at $T^* = 0.83$ (c.f. $T^* = 0.87$ liquid crystal-isotropic transition of Figure 5).

Comparing these transitions with those of the pure TsB system, it is seen that the solvent disrupts the crystallization of the TsB phase, extending the mesogenic hexagonal columnar phase to lower temperatures. The phase immiscibility is very pronounced, and the two phase system, with a TsB-rich nonstructured phase in equilibrium with a solvent-rich phase, is stable up to an upper critical solution temperature (UCST) close to $T^* = 1.30$ (an estimate, since simulations cannot be performed at the unknown critical composition). This UCST occurs well above the mesogenic to isotropic transition of the pure TsB phase. Below the UCST, with increasing temperature, the solvent concentration of the saturated TsB phase is seen to increase more rapidly than the TsB concentration of the saturated solvent phase. This behavior reflects an asymmetry in the phase composition dependence that, in turn, results from the dissimilarity of the component interactions. This unevenness also rationalizes the high interfacial tension between structured hexagonal columnar and solvent phases, previously suggested on the basis of the self-assembly simulations results.

In summary, the strong self-attractive nature of the type 1 solvents induces a phase split in the whole concentration range, apart from the very dilute regime. The incompatible nature of the TsB beads, chosen by design to drive microphase separation in the mesogenic phase, here compels bulk separation when type 1 beads are not locally constrained within a molecule.

7.2. Type 2 Bead Solvent. *7.2.1. Low Solvent Fraction and Full Composition Range.* The results of the low solvent fraction and full composition range study of the type 2 bead solvent mixtures have been reported previously;⁴¹ however, for completeness, they are presented in Figures 11 and 12, respectively. At low v_S , solvent beads are found localized in the interiors of the columns adjacent to the vertices. In the pure system, this region is seen from Figure 6 to have a lower average bead density and, hence, larger free accessible volume and cavities; consequently, the localization of free type 2 beads in this space leads to minimal disruption of type 3 self-interactions.

On reviewing the columnar swelling analysis in Figure 8, no expansion is seen over the range of miscibility. The capacity of the columns to accept free solvent molecules is, however, limited, and an excess solvent absorption would require inevitably a disruption of the honeycomb structure. Since the type 2 beads are soft-repulsive, such a column area expansion would impose a high energy penalty, that is, reduction of the type 1 interactions; thus, it appears to be unfavorable. At solvent fractions above $v_S = 0.061$, we observe the onset of immiscibility.

At higher v_S , phase coexistence between a TsB hexagonal columnar phase and solvent-rich phase of around $v_S = 0.675$ was observed. Examples of these coexisting phases are shown in Figure 12c–e. For all biphasic simulations, the interface between the solvent-rich phase and the TsB-rich phase exposes the

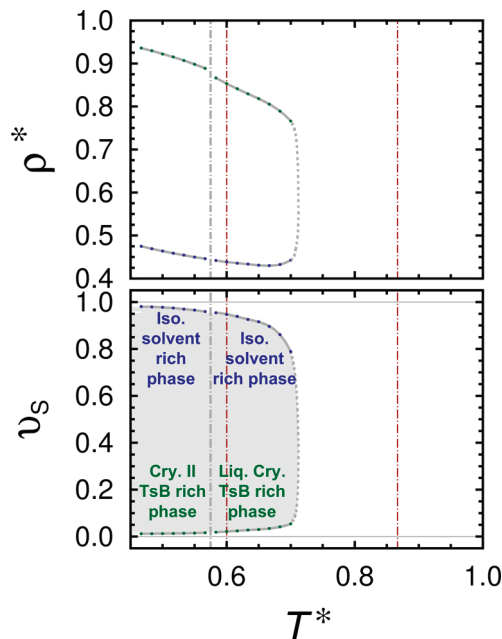


Figure 13. Plots of the phase densities, ρ^* , and phase solvent fractions, v_S , obtained by density analysis of biphasic MD simulations of a type 2 solvent and bolaamphiphile mixture. Gray vertical lines show the minimum temperature for which the columnar LC structure is present in one of the coexisting phases. Red vertical lines mark the minimum and maximum temperatures for which the pure $N_{\text{fix}} = 5$ TsB system exhibits columnar liquid crystalline behavior (c.f. Figure 5). Simulations were performed at $P^* = 0.78$.

hexagonal columnar ends, in contrast to the type 1 solvent mixtures. With this arrangement, there is minimal disruption to the hexagonal columns and limited removal of type 1 bead self-bonding than the alternative positioning of the solvent phase between columns. As an aside, this arrangement also permits a directed passage of solvent from the solvent-rich phase through the solvent-rich region of the columnar structure. In this configuration, the LC phase acts as a unique self-healing membrane⁴¹ whose thickness is controlled by composition rather than fixed by the molecular morphology, as is the case for lipid bilayer membranes. A larger illustration of this is given in Figure 3 of the Supporting Information.

At compositions above $v_S = 0.675$, complete miscibility is found. Toward the higher end of the composition range, $v_S = 0.675$ –1.000, amorphous micellar type structures were observed, as seen in Figure 12f and g. At the higher end of the range, monomer and dimer arrangements of TsB molecules in the solvent were predominant, as revealed in Figure 12h.

7.2.2. Biphasic Simulations. A coexistence study for the type 2 bead solvent system is summarized in the plots of the phase densities and solvent fractions presented in Figure 13. As with the type 1 solvent mixture, the temperature of the saturated TsB phase's crystalline to mesogenic columnar transition was lowered with respect to the pure system, to $T^* = 0.57$. In contrast, however, the UCST was found at roughly $T^* = 0.7$, a temperature below the mesogenic to isotropic transition of the pure phase. Consequently, type 2 bead solvents appear to reduce mesogenic phase stability at high temperatures. Moreover, we did not observe coexistence between a solvent-rich phase and a TsB-rich isotropic phase at higher temperatures. With increasing temperature, the composition, v_S , of the saturated solvent-rich phase

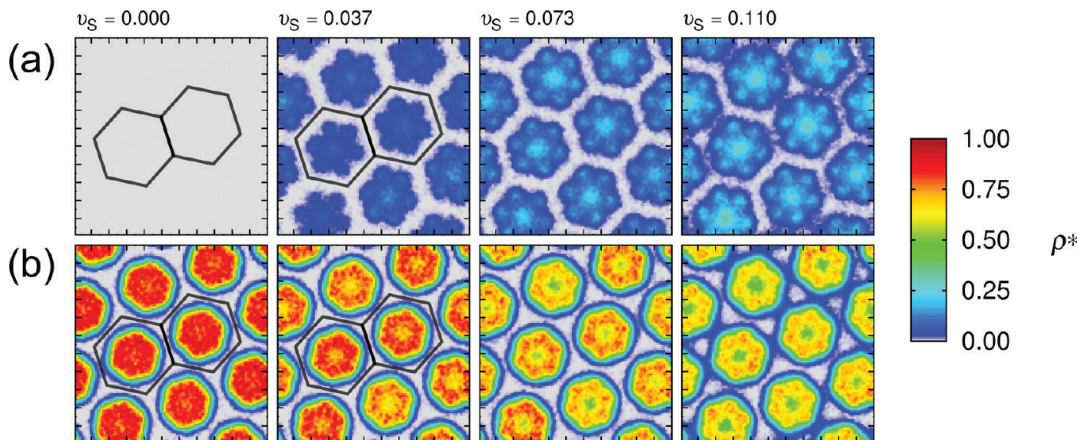


Figure 14. Director orthogonal density profiles, ρ^* , for the TsB and hydrophobic type 3 bead solvent mixture at low solvent concentration: (a) type 3 solvent beads and (b) type 3 TsB beads. The black line hexagons describe the positioning of the TsB rigid-rod units in the hexagonal columnar structures and are shown for reference only. Simulations were performed at $T^* = 0.67$ and $P^* = 0.78$.

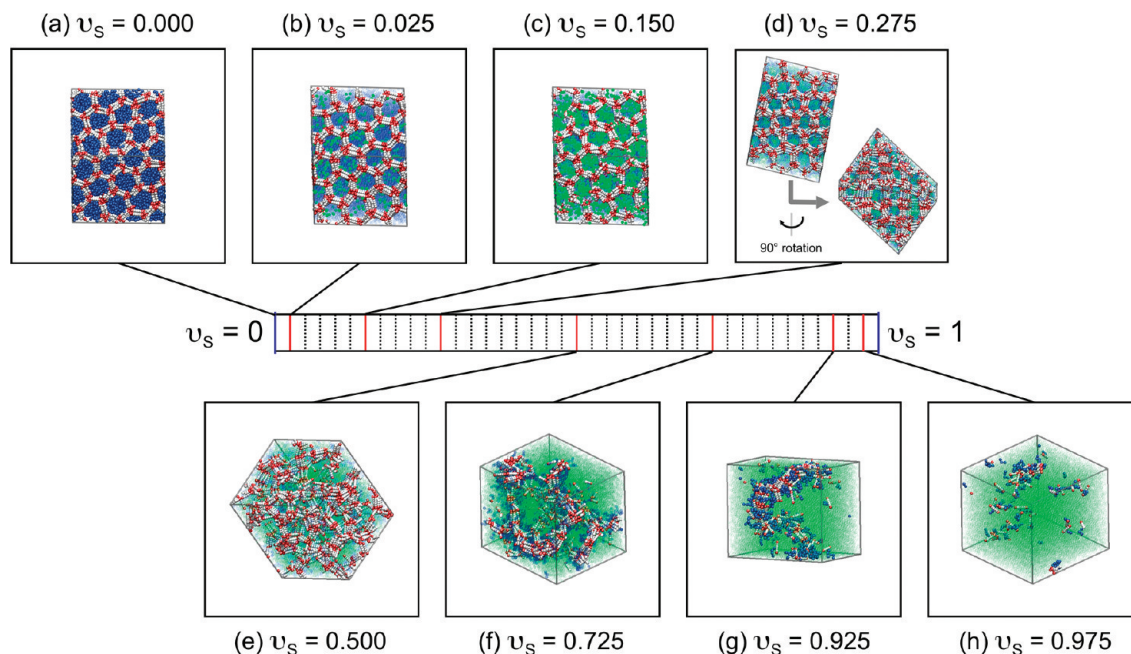


Figure 15. Snapshots taken from MD simulations at various overall solvent concentrations, v_S . The type 3 solvent is indicated with green beads. A single phase was observed for TsB molecule and type 3 bead solvent mixtures at all solvent fractions studied. Simulations were performed at $T^* = 0.67$ and $P^* = 0.78$.

decreases more dramatically than the v_S increase of the TsB-rich phase. This asymmetry is apparently due to component interaction asymmetry. Finally, it is worth pointing out the noticeably lower density of the solvent-rich saturated phase relative to the TsB phase, seen in Figure 13. This, in part, is attributed to the softly repulsive nature of type 2 beads. This is consistent with the overall benzene-like character of the solvent as compared with the hydrophilic-like polar type 1 beads.

7.3. Type 3 Bead Solvent. *7.3.1. Low Solvent Fraction.* In many ways, type 3 beads represent an intermediate between the two other bead types, and their mixture phase behavior might be expected to reflect this. The results of the low solvent concentration analysis are presented in Figures 8 and 14 and show otherwise. At low v_S , type 3 solvent beads are found to localize predominantly in the columns' centers and interior vertices, as

shown in the density orthogonal profiles in Figure 14. In contrast to type 1 and 2 solvent mixtures, at low v_S , there is a slight contraction of the columnar cross-sectional area, seen in Figure 8. This is rationalized by an increased type 3 bead density achieved relative to the noncontracted geometry, allowing the formation of additional attractions between beads. Eventually, repulsive core interactions between TsB type 1 beads in the columnar vertices limit this contraction, and although above $v_S = 0.049$, the hexagonal columnar structure persists, the cross-sectional area remains constant.

7.3.2. Full Composition Range. The results for the full type 3 bead solvent composition range are reported in Figure 15. In the range $v_S = 0.100$ – 0.275 , a transition occurs from a regular columnar structure to multiple slabs of a hexagonal columnar structure bridged by TsB rigid units across the columnar vertices.

An example of this is given in the $v_S = 0.275$ simulation snapshot of Figure 15d. To elucidate whether these slab structures were true equilibrium states, a simulation from an isotropic and homogeneous state at a composition of $v_S = 0.330$ was performed. Here, an amorphous network of rigid units bonding via the type 1 beads was formed, thus suggesting the bridged slab structures to be only metastable. On increasing v_S further by sequential conversion, an amorphous network similar to that obtained from the isotropic and homogeneous initiated simulation was obtained and is shown in Figure 15e. The sequential addition approach apparently led to some hysteresis of the hexagonal columnar structure phase into the network structure phase. This result, along with the trapping of the type 1 solvent mixtures in the metastable distorted columnar structures, shows some limitations to the use of sequential conversion. These in part could be circumvented by longer simulations; however, in many ways, it is more effective to use shorter run sequential addition simulations in parallel with other simulation strategies and phase analysis studies to piece together the full qualitative picture of the global phase behavior. At even higher v_S , a transition from the network structure to a wormlike, micellar-like solution was found, as shown in Figure 15g. Here, chains of the TsB rigid-unit sections were aligned together in strands bonded through the type 1 beads, leaving the lateral chains fully exposed to the surrounding solvent. At the highest solvent fractions studied some grouping of the TsB molecules remained; however, the fluid was mostly monomeric.

In contrast to the other mixtures, no distinct phase separation was observed for type 3 solvent mixtures at $T^* = 0.67$. Presumably, the weak self-interactions along with the increased mobility and size of the compatible side grafted chains allow for a single phase to be stable, regardless of the composition.

8. CONCLUSIONS

We have used a CG method to study phase behavior of a model TsB in the presence of three different solvents. At low concentrations, the solvents are absorbed into the hexagonal structure, but with different effects. Although the hydrophobic type 3 solvent tends to concentrate on the column core, it also tends to enhance the packing of the structure, decreasing the column area. Type 2 beads, compatible with the LC core, tend to fill in gaps in the structure without altering it. Hydrophilic type 1 solvents tend to migrate toward the vertices of the hexagons, effectively swelling the structure and eventually destabilizing the columns. In all cases, only a relatively small concentration of solvent may be added before the LC structure becomes saturated. These results are consistent with the limited experimental data available for these systems¹⁹ and suggest the limits and conditions at which solvents or colloidal particles can be embedded in these honeycomb LC matrices.

All three solvent mixtures behave differently at higher concentrations. Depending on the nature of the solvent, the system may or may not experience a phase split, with one phase exhibiting a significant order while the coexisting phase is predominantly supersaturated solvent.

We have not seen evidence of solvent-induced transitions to any of the alternative equilibrium mesophases observed in pure-phase simulations of TsB models with longer chain lengths. For example, although increased type 3 solvents compositions could viably induce transformation from hexagonal columnar structures to lamellar phases, this was not seen. Perhaps unsurprisingly, chain connectivity is more important here than the system

particle type fractions. The mobility of the solvent and its detachment to the LC core result in unique phases and interfaces in a rather large temperature domain which include wormlike micelles and self-healing LC membranes. These structures may be fine-tuned both by design of the participating molecules but, maybe, more importantly by changes in concentration.

It is clear that the results obtained are generic in nature because the TsB structures generated share commonalities with recently studied silica–surfactant systems,⁴² block copolymers,⁴³ and star–polyphilic systems,⁴⁴ to name a few. One would expect that exploring the phase space of mixtures of these systems with solvents would produce related results.

■ ASSOCIATED CONTENT

S Supporting Information. Details of the calamitic bolaamphiphile simulations, simulation details, and further snapshots of some mixture configurations are available as Supporting Information. This material is available free of charge via the Internet at <http://pubs.acs.org>.

■ AUTHOR INFORMATION

Corresponding Author

*E-mail: e.muller@imperial.ac.uk.

■ ACKNOWLEDGMENT

Financial support for this work has been given by the U.K. Engineering and Physical Sciences Research Council (EPSRC), Grant EP/E016340, “Molecular Systems Engineering”. Some figures were drawn using VMD.⁴⁵

■ REFERENCES

- (1) Tschierske, C. *J. Mater. Chem.* **1998**, *8*, 1485–1508.
- (2) Goltner, C. G.; Antonietti, M. *Adv. Mater.* **1997**, *9*, 431–436.
- (3) Wan, Y.; Zhao, D. *Chem. Rev.* **2007**, *107*, 2821–2860.
- (4) Patti, A.; Mackie, A. D.; Siperstein, F. R. *J. Mater. Chem.* **2009**, *19*, 7848–7855.
- (5) Fuhrhop, J. H.; Wang, T. *Chem. Rev.* **2004**, *104*, 2901–2938.
- (6) Kato, T.; Mizoshita, N.; Kishimoto, K. *Angew. Chem., Int. Ed.* **2006**, *45*, 38–68.
- (7) Tschierske, C. *Chem. Soc. Rev.* **2007**, *36*, 1930–1970.
- (8) Cheng, X. H.; Das, M. K.; Baumeister, U.; Diele, S.; Tschierske, C. *J. Am. Chem. Soc.* **2004**, *126*, 12930–12940.
- (9) Hildebrandt, F.; Schroter, J. A.; Tschierske, C.; Festag, R.; Kleppinger, R.; Wendorff, J. H. *Angew. Chem., Int. Ed. Engl.* **1995**, *34*, 1631–1633.
- (10) Crane, A. J.; Martínez-Veracoechea, F. J.; Escobedo, F. A.; Müller, E. A. *Soft Matter* **2008**, *4*, 1820–1829.
- (11) Bates, M.; Walker, M. *Soft Matter* **2009**, *5*, 346–353.
- (12) Lintuvuori, J. S.; Wilson, M. R. *Phys. Chem. Chem. Phys.* **2009**, *11*, 2116–2125.
- (13) Horsch, M. A.; Zhang, Z.; Glotzer, S. C. *Phys. Rev. Lett.* **2005**, *95*, 056105.
- (14) Horsch, M. A.; Zhang, Z.; Glotzer, S. C. *Nano Lett.* **2005**, *6*, 2406–2413.
- (15) Nguyen, T. D.; Glotzer, S. C. *ACS Nano* **2010**, *4*, 2585–2594.
- (16) Horsch, M. A.; Zhang, Z.; Glotzer, S. C. *Soft Matter* **2009**, *6*, 945–954.
- (17) Wilson, M. R. *Chem. Soc. Rev.* **2007**, *36*, 1881–1888.
- (18) Sauer, C.; Diele, S.; Lindner, N.; Tschierske, C. *Liq. Cryst.* **1998**, *25*, 109–116.

- (19) Qi, H.; Lepp, A.; Heiney, P. A.; Hegmann, T. *J. Mater. Chem.* **2007**, *17*, 2139–2144.
- (20) Nielsen, S. O.; Lopez, C. F.; Srinivas, G.; Klein, M. L. *J. Phys.: Condens. Matter* **2004**, *16*, R481–R512.
- (21) McCullagh, M.; Prytkova, T.; Tonzani, S.; Winter, N. D.; Schatz, G. C. *J. Phys. Chem. B* **2008**, *112*, 10388–10398.
- (22) Müller, E. A.; Gelb, L. D. *Ind. Eng. Chem. Res.* **2003**, *42*, 4123–4131.
- (23) Shinoda, W.; Devane, R.; Klein, M. L. *Mol. Simul.* **2007**, *33*, 27–36.
- (24) (a) Izvekov, S.; Voth, G. A. *J. Phys. Chem.* **2005**, *109*, 2469–2473. (b) Izvekov, S.; Voth, G. A. *J. Chem. Phys.* **2005**, *123*, 134105.
- (25) Hansen, J. P.; McDonald, I. R. *Theory of Simple Liquids*, 3rd ed.; Academic Press: London, 2006.
- (26) Gray, C. G.; Gubbins, K. E. *Theory of Molecular Fluids*; Oxford University Press: Oxford, 1984.
- (27) Müller, E. A.; Gubbins, K. E. *Ind. Eng. Chem. Res.* **2001**, *40*, 2193–2211.
- (28) Kontogeorgis, G. M.; Folas, G. K. *Thermodynamic Models for Industrial Applications: From Classical and Advanced Mixing Rules to Association Theories*; Wiley, New York, 2010.
- (29) Marrink, S. J.; Risselada, H. J.; Yefimov, S.; Tieleman, D. P.; de Vries, A. H. *J. Phys. Chem. B* **2007**, *111*, 7812–7824.
- (30) Shinoda, W.; DeVane, R.; Klein, M. L. *J. Phys. Chem. B* **2010**, *114*, 6836–6849.
- (31) Grest, G. S.; Lacasse, M. D.; Kremer, K.; Gupta, A. M. *J. Chem. Phys.* **1996**, *105*, 10583–10594.
- (32) Weeks, J. D.; Chandler, D.; Andersen, H. C. *J. Chem. Phys.* **1971**, *54*, 5237–5247.
- (33) Kölbel, M.; Beyersdorff, T.; Cheng, X. H.; Tschierske, C.; Kain, J.; Diele, S. *J. Am. Chem. Soc.* **2001**, *123*, 6809–6818.
- (34) Cheng, X. H.; Prehm, M.; Das, M. K.; Kain, J.; Baumeister, U.; Diele, S.; Leine, D.; Blume, A.; Tschierske, C. *J. Am. Chem. Soc.* **2003**, *125*, 10977–10996.
- (35) Kieffer, R.; Prehm, M.; Pelz, K.; Baumeister, U.; Liu, F.; Hahn, H.; Lang, H.; Ungar, G.; Tschierske, C. *Soft Matter* **2009**, *5*, 1214–1227.
- (36) Shi, W.; Johnson, J. K. *Fluid Phase Equilib.* **2001**, *187*, 171–191.
- (37) de Miguel, E.; del Rio, E. M.; Blas, F. J. *J. Chem. Phys.* **2004**, *121*, 11183–11194.
- (38) Gelb, L. D.; Müller, E. A. *Fluid Phase Equilib.* **2002**, *203*, 1–14.
- (39) Martínez-Veracoechea, F. J.; Müller, E. A. *Mol. Simul.* **2005**, *31*, 33–43.
- (40) For a recent review, see: Smith, W. *Mol. Simul.* **2006**, *32*, 933–1121; www.ccp5.ac.uk/DL_POLY/ (accessed March 11, 2011).
- (41) Crane, A. J.; Müller, E. A. *Faraday Discuss.* **2010**, *144*, 187–202.
- (42) Patti, A.; Mackie, A. D.; Zelenak, V.; Siperstein, F. R. *J. Mater. Sci.* **2009**, *19*, 724–732.
- (43) Alsunaidi, A.; den Otter, W. K.; Clarke, J. H. R. *J. Chem. Phys.* **2009**, *130*, 124910.
- (44) Kirkensgaard, J. J. K.; Hyde, S. *Phys. Chem. Chem. Phys.* **2009**, *11*, 2016–2022.
- (45) Humphrey, W.; Dalke, A.; Schulten, K. *J. Mol. Graphics* **1996**, *14*, 33–38.